Transport through Redox-Active Ru-Terpyridine Complexes Integrated in Single Nanoparticle Devices

Max Mennicken[1,2], Sophia K. Peter[3], Corinna Kaulen[3,4*], Ulrich Simon[3], Silvia Karthäuser[1*]

[1]Peter Grünberg Institut (PGI-7) and JARA-FIT, Forschungszentrum Jülich GmbH, Jülich 52425, Germany.

*E-Mail: s.karthaeuser@fz-juelich.de

[2]RWTH Aachen University, Aachen 52062, Germany

[3]JARA – FIT and Institute of Inorganic Chemistry, RWTH Aachen University, Aachen 52074, Germany

[4]Faculty of Medical Engineering and Applied Mathematics, FH Aachen, University of Applied Science, 52428 Jülich, Germany

*E-Mail: kaulen@fh-aachen.de

Abstract

Transition metal complexes are electrofunctional molecules due to their high conductivity and their intrinsic switching ability involving a metal-to-ligand charge transfer. Here, a method is presented to contact reliably a few to single redox-active Ru-terpyridine complexes in a CMOS compatible nanodevice and preserve their electrical functionality. Using hybrid materials from 14 nm gold nanoparticles (AuNP) and bis-{4'-[4-(mercaptophenyl)-2,2';6',2''-terpyridine]}-ruthenium(II) complexes a device size of 30^2 nm^2 inclusive nanoelectrodes is achieved. Moreover, this method bears the opportunity for further downscaling. The Ru-complex AuNP devices show symmetric and asymmetric current *versus* voltage curves with a hysteretic characteristic in two well separated conductance ranges. By theoretical approximations based on the single-channel Landauer model the charge transport through the formed double-barrier tunnel junction is thoroughly analyzed and its sensibility to the molecule/metal contact revealed. It can be verified that tunneling transport through the HOMO is the main transport mechanism while decoherent hopping transport is present to a minor extent.

1. Introduction

Single molecule and large area molecular electronics are expected to be promising elements with specifically tunable functions to supplement CMOS-based circuits.[1-3] Admittedly, the integration of molecular devices is a considerable challenge, due to the need of nano-gapped electrodes with high precision and the demanding control of molecule-metal contacts as well as the molecular properties within the nanoelectrode gaps. It is especially challenging, e. g., to wire reliably short, switchable molecules to electrodes in order to achieve a considerable device conductance, while at the same time their switching ability is preserved. In this regard, light or voltage-driven molecular switches, which exhibit only minor changes in conformation, are considered as preferred candidates for the integration into solid state electronic devices.

In the last years molecule junctions based on transition metal complexes (TMC) attracted remarkable attention.[4-8] The progress in this area is based on an enlarged understanding of their fundamental conduction mechanism and switching ability. TMC show interesting features distinct from those of organic molecules originating mainly from metal-ligand dπ-pπ interactions.[9,10] One consequence is the high conductivity of TMC wires, verified by relatively small decay constants of β_{TMC} = 0.9 – 1.1 nm^{-1} measured in solution, which are attributed to a thermally activated hopping conduction.[11,12] In comparison to these TMC wires, organic oligomers exhibit higher decay constants, e. g., oligo-(phenylene-ethynylene) wires (OPE) β_{OPE} = 2.1 nm^{-1}, oligo-phenylenes β_{phen} = 4.4 nm^{-1}, or alkane chains β_{alk} = 7.6 nm^{-1}.[8,13-15] Generally it is assumed that the characteristic transport mechanism for these organic molecules/oligomers with a length < 3 nm is tunneling transport. The redox properties of TMC in solution are well confirmed by cyclic voltammetry and fluorescence-lifetime measurements.[9,16,17] Moreover, TMC monolayers were used to form light or voltage-driven solid state devices which show a clear switching behavior.[18-20] In addition, the switch-on threshold voltage of thiol-tethered Ru(II) terpyridine complexes embedded in a *n*-alkanethiol monolayer was determined in the range 1.70 – 1.75 V using a scanning tunneling microscope.[21] However, it remains

a complex task to test the reversible switching ability of a single TMC in a CMOS compatible, solid state device geometry.

For this purpose, hybrid materials from gold nanoparticles (AuNP) and TMC are especially interesting, since they bear the possibility to control the assembly of the AuNP within a device configuration, while the intrinsic photophysical, electrochemical, or electronic properties of the functional complexes can be addressed.[22] This approach is in line with our already successfully applied method to investigate nanodevices based on single ligand-stabilized AuNP to probe the transport properties of the ligand molecules.[23-26] In this regard, suitable nanodevices are required which offer gaps between nanoelectrodes in the size range of the molecular building blocks, i.e. in the few nanometer range. We have already shown that it is possible to fabricate nanodevices with gap sizes down to 3 nm by electron beam lithography (EBL) in a lift-off process.[27] Furthermore, we recently introduced a process to produce nanoelectrode pairs composed of different metals with gap sizes down to 10 nm. The nanoelectrodes are again defined by EBL while in a modified lift-off process a self-aligned Al_2O_3 hard mask is used to control the nanogap size.[24,26,28] The resulting heterometallic nanoelectrode pairs are suitable for the directed assembly of nanoelements or molecules equipped with two different, adequately selected anchor groups on opposite sites.[25]

The molecules under consideration in this work, the twofold positively charged bis-{4'-[4-(mercaptophenyl)-2,2';6',2''-terpyridine]}-ruthenium(II) complex ($Ru(MPTP)_2$) molecules with two chloride counterions, form the ligand shell around the AuNP, that are immobilized between nanoelectrodes. In this setup, the gap between the nanoelectrodes advantageously does not need to be as small as the molecule in order to study molecular properties. However, we are employing AuNPs with a size of 14 nm and nanoelectrodes with a separation of 10 nm and thus, assemble single $Ru(MPTP)_2$-AuNP in between heterometallic nanoelectrodes to form a nanodevice. Consequently, the transport properties of a few or even single $Ru(MPTP)_2$-complexes are obtained.

2. Experimental Methods

2.1. Chemical Synthesis and Analysis

2.1.1. Materials. The following chemicals were purchased from Sigma-Aldrich Chemie GmbH and used as received: hydrogen tetrachloroaurate(III) trihydrate ($HAuCl_4 \cdot 3H_2O$), trisodium citrate dihydrate ($C_6H_5Na_3O_7 \cdot 2H_2O$), methylthiobenzaldehyde (C_8H_8OS), 2-acetylpyridine (C_7H_7NO), $RuCl_3 \cdot xH_2O$, acetic anhydride ($C_4H_6O_3$), acetic acid ($C_2H_4O_2$), dimethyl sulfoxide (C_2H_6OS, DMSO), tetrahydrofuran (C_4H_8O, THF). Aqua regia and copious amounts of ultrapure water (< 55 nS cm^{-1}) were used to clean glassware prior to use. Citrate stabilized AuNP (approx. 13 nm in diameter) were prepared by the Turkevich method.[29] Synthesis of 4'-mercaptophenyl-2,2':6',2"-terpyridine (MPTP) and its complexes was performed under argon using Schlenk technique. MPTP, $RuCl_2(DMSO)_4$, and MPTP-AuNP were synthesized as previously published.[26,30,31] Details of the synthesis and analysis of 4'-[4-(acetylthio)phenyl]-2,2':6',2''-terpyridine (MPTP-SAc) and the complex $RuCl_2$(DMSO)MPTP-SAc are given in the Supporting Information: 1. Chemical Synthesis and Analysis, Figures S1-S4.

2.1.2. Synthesis of Ru(MPTP)(MPTP-SAc)-functionalized AuNP. Ru(MPTP)(MPTP-SAc)-AuNPs were prepared starting from MPTP-AuNP by reaction with $RuCl_2$(DMSO)(MPTP-SAc) in a mixture of acetic acid and water (1:5, (v:v)). 6.3 mg of $RuCl_2$(DMSO)(MPTP-SAc) were dissolved in 1 mL of acetic acid solution and 250 µl of this solution added to 5 mL of MPTP-AuNP in acetic acid. The solution was kept overnight at 60 °C, then the Ru(MPTP)(MPTP-SAc)-AuNP were centrifuged 3 times at 10.000 rpm/15 min and redispersed in water. After the last centrifugation step no traces of Ru-complex were detectable in the UV-vis spectrum of the supernatant. The purified Ru(MPTP)(MPTP-SAc)-AuNP were analyzed by scanning electron microscopy in transmission mode (SEM-T), UV-vis absorption spectra, Fourier transform infrared spectroscopy (FT-IR) and atomic absorption spectroscopy (AAS).

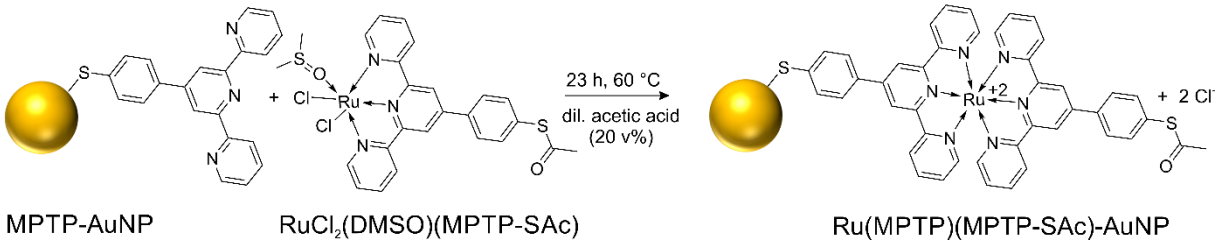

Figure 1. Schematic illustration of the Ru(MPTP)(MPTP-SAc)-AuNP synthesis

2.1.3. Nanoparticle Characterization. UV−vis absorption spectra were conducted with a JASCO V-630 spectrophotometer. A Malvern Zetasizer Nano S, He−Ne laser (λ = 633 nm, P = 4 mW, ϑ = 173°) was used to perform dynamic light scattering (DLS) measurements and ζ-potential measurements in order to obtain the hydrodynamic radii and the polydispersity index (PDI) of the AuNP dispersions. FT-IR spectra were collected from a FT-IR spectrometer (Vertex 70, Bruker Optics) equipped with a MCT detector (spectral resolution 4 cm^{-1}). SEM-T was performed with a high-resolution field emission SEM (LEO/ZEISS Supra 35 VP, Oberkochen, Germany). ^{1}H- and ^{13}C-NMR spectra were collected form a Bruker Avance II 400 (1H: 400 MHz, 13C: 100 MHz; T = 23° C). Chemical shifts are given in ppm against TMS (tetramethylsilane) and refer to the rest proton signals of either d-DMSO or CD_2Cl_2. AAS measurements were recorded on an AA-6200 from Shimadzu. For that, samples were dissolved in aqua regia.

2.2. Nanodevice Fabrication

2.2.1. Nanoelectrode Fabrication. Nanoelectrode structures were fabricated according to a recently presented method by electron beam lithography in a lift-off process.[26] The design of the electrode structure is given in Supporting Information Figure S5. Every sample, foreseen for the immobilization of the ligand covered AuNPs, is equipped with 12 nanoelectrode pairs consisting of an AuPd electrode and a Pt electrode with a 10 nm gap in between.

2.2.2. Assembly of Ru(MPTP)$_2$-AuNP Devices. In order to immobilize single Ru(MPTP)(MPTP-SAc)-AuNP in nanogaps, a droplet of the diluted dispersion of Ru(MPTP)(MPTP-SAc)-AuNP in deionized

water (5 μl) was deposited on the nanoelectrode section of the sample. After 5 minutes of incubation this droplet was blown off with a nitrogen stream. Thereafter, the sample was covered with 25 wt % ammonium solution for 1 minute in order to hydrolyze *in situ* the acetyl-protected thiol groups of MPTP-SAc, resulting in a $Ru(MPTP)_2$-AuNP device. This is merely possible after forming the nanoparticle device, as it would lead to an immediate dimerization of Ru(MPTP)(MPTP-SAc)-AuNP in solution. To clean the sample from all residues, it was finally rinsed with deionized water or ethanol and blown dry with nitrogen.

2.3. Nanodevice Characterization

Cyclic current versus voltage (*I/U*) measurements were carried out in a probe station equipped with tungsten probes. A more detailed description of this setup and the connection procedure was recently described.[26] Voltage sweeps were applied to the AuPd electrode with a Keithley 6430 sub-femtoamp remote source meter while the Pt electrode was connected to ground. Current-voltage characteristics were recorded under ambient conditions at room temperature. After all transport measurements were completed, the samples were finally imaged using an SEM.

3. Results and Discussion

3.1. Synthesis and Characterization of Ru(MPTP)(MPTP-SAc)-AuNP

Ru(MPTP)(MPTP-SAc)-AuNP were prepared by ligand complexation of the MPTP-AuNP with the Ru-precursor, $RuCl_2$(DMSO)(MPTP-SAc), according to Figure 1. The Ru-precursor was obtained in good yield by reaction of MPTP-SAc and $RuCl_2(DMSO)_4$ in THF (56%). Acetyl protection of the precursor was performed in order to inhibit the reaction of the free thiol group with the AuNP surface during complex formation. The reaction of MPTP-AuNP and $RuCl_2$(DMSO)(MPTP-SAc) was carried out in aqueous acetic acid, which stabilizes the MPTP-AuNP as single particles in solution, while the temperature of 60°C results in a reasonable reaction time of 24 h.[32] After removing excess Ru-precursor, the Ru(MPTP)(MPTP-SAc)-AuNP are stable as single particles in neutral water, as also indicated by the hydrodynamic radius, d_H, and the PDI (Table 1). These data verify successful complex formation and electrostatic stabilization due to the positively charged Ru-complexes. Comparing the UV-vis spectra of MPTP-AuNP and Ru(MPTP)(MPTP-SAc)-AuNP reveals no change in the plasmon peak maximum due to complexation (Figure 2a). The SEM-T images of the Ru(MPTP)(MPTP-SAc)-AuNP show mainly spherical particles with an average size of 14 ± 1.4 nm. Some larger particles may stem from aggregation or Ostwald ripening of the AuNP during the long reaction time at elevated temperature (Figure 2b). The FT-IR spectrum exhibits all peaks of the MPTP ligand and in addition the ν(C=O) vibration of the acetyl group protecting the thiol (Figure 3). The Au- and the Ru-content of the samples was determined by AAS (Table S1, Supporting Information) and we deduced that at maximum 62% of the initially present MPTP-ligands on the AuNP surface were transformed to Ru(MPTP)(MPTP-SAc)-complexes.

Table 1. Comparison of MPTP-AuNP (in aqueous AcOH) and Ru(MPTP) (MPTP-SAc)-AuNP (in H_2O).[26]

	λ_{max} [nm]	d_H [nm]	PDI	Size [nm]
MPTP-AuNP	533	20.0 ± 0.2	0.32 ± 0.04	13 ± 2.0
Ru(MPTP)(MPTP-SAc)-AuNP	533	33.2 ± 0.3	0.47 ± 0.01	14 ± 1.4

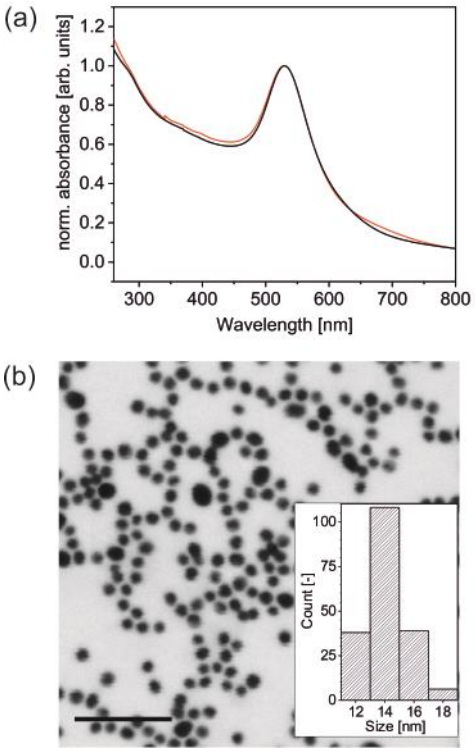

Figure 2. (a) UV-vis spectra of MPTP-AuNP (black) and Ru(MPTP)(MPTP-SAc)-AuNP (red). Additional UV-vis spectrum of the Ru(MPTP)(MPTP-SAc)-complex, see Figure S6, Supporting Information. (b) SEM-T image of Ru(MPTP)(MPTP-SAc)-AuNP (scale bar = 100 nm). Inset: corresponding histogram displaying the nanoparticle size distribution.

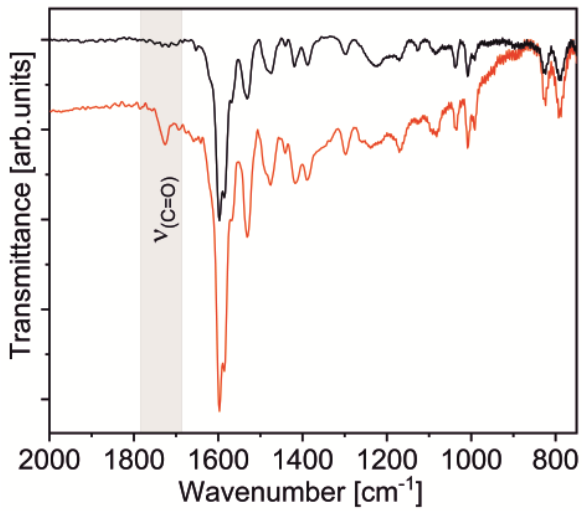

Figure 3. FT-IR spectra of MPTP-AuNP (black) and Ru(MPTP)(MPTP-SAc)-AuNP (red).

3.2. Electrical Properties of Single Ru(MPTP)$_2$-AuNP Devices

Single Ru(MPTP)(MPTP-SAc)-AuNP with a diameter of 14 nm have been immobilized between heterogeneous nanoelectrode pairs (metal combination AuPd and Pt) with a gap size of about 10 nm (Figure 4a). The thus formed solid-state junctions are based on Ru(MPTP)$_2$-AuNP which result as a consequence of the Ru(MPTP)(MPTP-SAc)-AuNP hydrolysis during the immobilization procedure. The electrical behavior of the Ru(MPTP)$_2$-AuNP devices has been tested by cyclic current *versus* voltage (*I*/*U*) measurements in the voltage range -1.5 V < *U* < +1.5 V. Functional devices are usually characterized by more than 30 sweeps and in extraordinary cases by up to 100 sweeps pointing to a remarkable electrical robustness of these double-barrier tunnel junctions, AuPd/Ru(MPTP)$_2$/AuNP/Ru(MPTP)$_2$/Pt. In Figure 4b the *I*/*U*-data characteristic for such a single Ru(MPTP)$_2$-AuNP solid-state device are plotted in a heat map (Figure 4b) and the corresponding histogram of the current values at ±1 V is shown in Figure 4c. It should be noted that all employed nanogaps have been electrically characterized in their pristine state after fabrication and before immobilization of the AuNPs, to rule out artifacts. Only nanogaps with an isolation resistance > 10 TΩ were used for further experiments. Measurements showing *I*/*U* curves on empty nanogaps are given for reference purposes in Figure S7, Supporting Information. Furthermore, it is necessary to note that all SEM images of nanoparticle devices were taken after electrical characterization in order to prevent any destruction of the functional molecules and to avoid charging of the device through the electron beam.

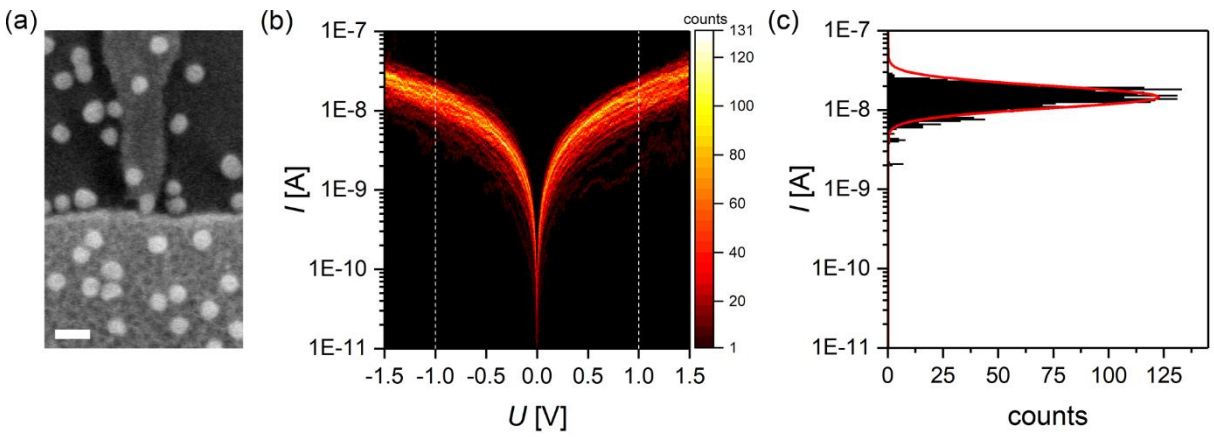

Figure 4. (a) SEM image of a single Ru(MPTP)$_2$-AuNP located between an AuPd and a Pt nanoelectrode forming a solid-state device (scale bar: 30 nm). (b) Heat map (x-bin = 10 mV, y-bin = 0.02 log(I)) and (c) current histogram (at ±1 V) displaying the *I*/*U*-measurements through a single nanoparticle device.

The heat map in Figure 4b shows data from 55 *I/U* cycles. A peak fit to the corresponding histogram (Figure 4c) reveals a device conductance of 14 ± 3 nS. By applying this method to the data gathered from 7 devices we determined 11 conductance values. That is, some devices show a low conductance value, jump after a while to a considerably higher one and stay at this value for the rest of the measurement. Thus, more than one conductance value is deduced from one device. In Figure 5a the conductance values at ±1 V resulting for the single Ru(MPTP)$_2$-AuNP devices are given in ascending order. They can be categorized in two groups, high conductivity devices and low conductivity devices. Both groups differ in their average conductance by nearly two orders of magnitude. These observations lead us to the tentative assumption that the mean higher conductance value of 14 nS can be attributed to a Ru(MPTP)$_2$-AuNP device with an envisaged strong coupling between the thiol linker groups and Au, AuPd or Pt, respectively, due to the formation of chemical bonds at each molecule/metal interface (Figure 5b)**.** The mean lower conductance value of 0.36 nS might indicate that the *in situ* hydrolysis of the protecting groups has not been completed and a number of acetyl groups remain at the interfaces, as observed for acetyl-protected Ru-complex wires.[8] The thus formed Ru(MPTP)(MPTP-SAc)-AuNP devices (Figure 5b) would exhibit a considerably reduced conductance due to an increased tunneling distance and a weak coupling between the acetyl groups and the electrodes. The resulting conductance values are in line with the conductance of 2.1 nS obtained for methyl protected Ru(MPTP-SMe)$_2$-complexes in metal/single molecule/metal junctions using a non-contact *I*(*z*)-method.[11,12] In the latter case the weaker coupling of the methylthioether linker group compared to the thiol linker group employed here can be regarded as reason for a reduced conductance through the Ru-terpyridine complex.

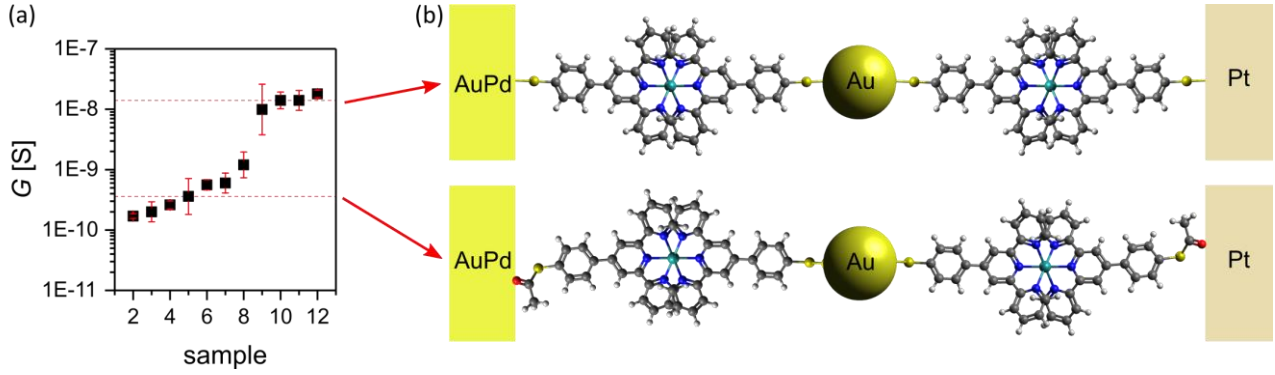

Figure 5. (a) Experimental conductance statistics. The error bars given for the individual conductance values correspond to the full width at half maximum deduced from the corresponding current histograms at ±1 V (like given in Figure 4c). (b) Schematic displaying two possible edge cases of the single Ru(MPTP)$_2$-AuNP device structure with complete hydrolysis (upper part) and without hydrolysis of the protecting acetyl groups resulting in Ru(MPTP)(MPTP-SAc)-AuNP devices (lower part).

Remarkably, distinct hysteretic current *versus* voltage characteristics result from single Ru(MPTP)$_2$-AuNP devices, if the *I*(*U*)-curves are plotted on a linear scale. In Figure 6 representative hysteresis curves are shown for high and low conductance devices, respectively. While the *I*(*U*)-curve of the high conductance device, attributed to a single Ru(MPTP)$_2$-AuNP junction, is symmetric, the *I*(*U*)-curve given in Figure 6b is asymmetric. One possible explanation for this asymmetry is an asymmetric double-barrier tunnel junction, like AuPd/Ru(MPTP)$_2$/AuNP/Ru(MPTP)(MPTP-SAc/Pt. This corresponds to an incomplete hydrolysis of the thiol protecting acetyl groups in one of the tunneling junctions and would cause directly different resistances of the two tunnel junctions on the left and the right side of the AuNP (see schematic in Figure 5b for the device geometry). Consequently, it can be deduced that the group of single AuNP devices with lower conductance comprises symmetric as well as asymmetric devices with at least an acetyl group remaining at one molecule/metal interface (for simplicity they are all abbreviated as Ru(MPTP)(MPTP-SAc)-AuNP devices in the following).

The hysteretic *I*/*U*-characteristic indicates that single nanoparticle devices based on switching transition metal complexes as ligands have the potential to be used in molecular memories. The

maximum ratio between the On-state current (ascending voltage) and the Off-state current (descending voltage) is roughly 1.5 and it is reached in the negative bias regime for the high conductance as well as the low conductance device. This On/Off ratio of 1.5 is comparable to values of 1.07 and 3 obtained for monolayer-based molecular devices using $Ru(MPTP)_2$-complexes as switching elements.[18,19] However, we like to point out that these monolayer based devices have usually sizes of tens of µm (for example: 25^2 μm^2) while our single $Ru(MPTP)_2$-AuNP device covers an area of 30^2 nm^2 with the electrodes included.

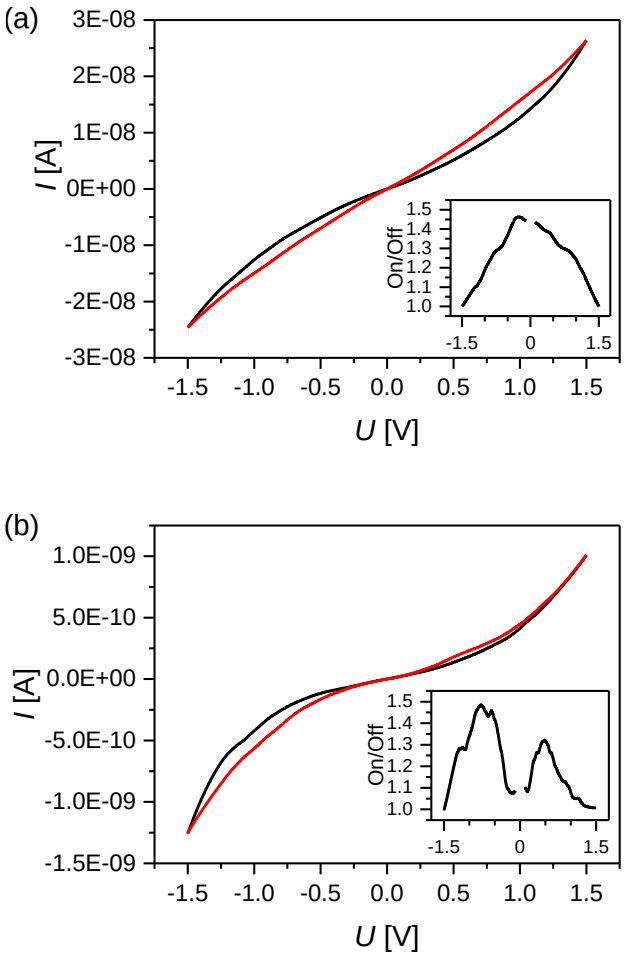

Figure 6. Hysteretic current *versus* voltage characteristics, ascending (red) and descending (black) *I*/*U*-curves (a) high conductance device, (b) low conductance device. Inset shows the On/Off ratio in each case.

3.3. Transition Voltage Spectroscopy

Transition voltage spectroscopy (TVS) is a means to further analyze the transport characteristics in the medium bias regime of tunneling junctions.[15,33,34] A transition from coherent tunneling to Fowler-Nordheim tunneling through a triangular barrier is indicated by a minimum, U_T, in the $\ln(I/U^2)$ *versus* $1/U$ plot (Fowler-Nordheim plot) and corresponds to the energy offset of the molecular frontier orbitals with respect to E_F of the metallic electrodes. Equivalent to Fowler-Nordheim plots (Figure S8, Supporting Information), but simpler to handle, are plots of abs(U^2/I) versus U (Figure 7) as recently reported.[34] Here the maximum of the curve corresponds to the transition voltage, U_T, and the results of both approaches are the same. For Ru(MPTP)$_2$-AuNP or Ru(MPTP)(MPTP-SAc)-AuNP devices with high or low conductance, respectively, clear maxima were obtained which allowed to deduce the transition voltage. The mean values determined for the high and the low conductance devices are $U_{T,High}$ = 1.17 ± 0.08 V and $U_{T,Low}$ = 0.85 ± 0.10 V (Figure 7). It is apparent that there is a noticeable difference in the transition voltages $U_{T,High}$ and $U_{T,Low}$. The finding of a higher transition voltage for the high conductance device is counter-intuitive, and the experimental values obtained here are considerably higher than transition voltages given for Ru-complex wires as small as 0.25 eV.[35] However, transition voltages deduced from a double-barrier tunnel junction need to be interpreted in a different way.

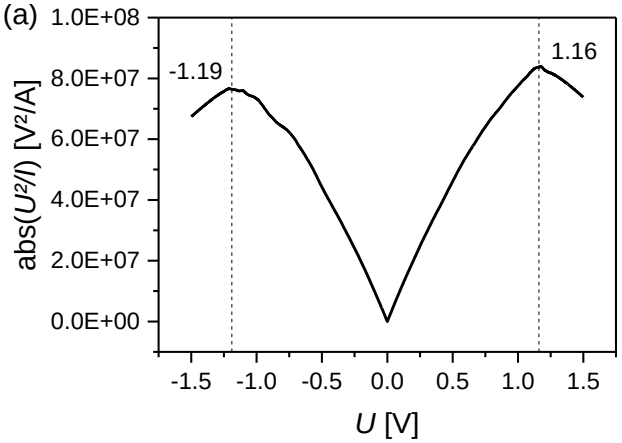

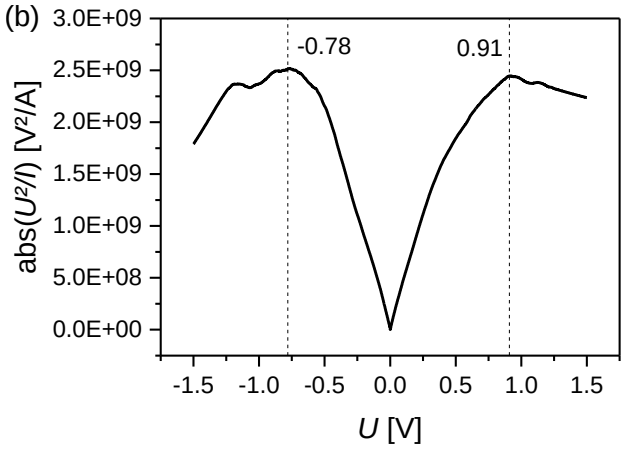

Figure 7. Transition voltage spectroscopy (a) $Ru(MPTP)_2$-AuNP device (average of 5 voltage sweeps), (b) Ru(MPTP)(MPTP-SAc)-AuNP device (average of 30 voltage sweeps). The values of the respective U_T are indicated in the diagram.

It is imperative to consider the architecture of the double-barrier tunnel junction, which is quite different from, for example, a STM set-up with a molecule strongly coupled to the substrate and separated from the tip by a vacuum gap, often used to determine U_T.[15] According to DFT analysis the HOMO of TMC, especially Ru-complexes, can be regarded as the major conductive pathway.[5,35] Likewise, $Ru(MPTP)_2$ is expected to show hole transport since the HOMO is reported to be located close to the E_F (metal).[9,13] In the case of contacting a single Ru-complex between two electrodes, that is, a single tunneling barrier, the energy offset between E_F and HOMO ($\Delta E_H = E_F$ – HOMO) determines the transition from coherent tunneling to Fowler-Nordheim tunneling. However, in a symmetric double-barrier tunnel junction the applied voltage, U, drops over two consecutive tunneling barriers and thus, needs to be twice U_T of a single tunneling barrier (see Figure 8). Furthermore, a strong coupling between the thiol anchor groups and the respective metal can be assumed for high conductance devices, AuPd/$Ru(MPTP)_2$/AuNP/$Ru(MPTP)_2$/Pt (Figure 5b and 8a), so that overall four almost equivalent molecule/metal interfaces result. Since the thiol/metal junctions are the parts of the $Ru(MPTP)_2$-AuNP devices with the highest resistance the applied voltage is assumed to drop mainly in equivalent amounts at these four interfaces. This leads to a potential drop of $eU/4$ at each

interface (Figure 8a). In this scenario the transition voltage obtained for a single Ru(MPTP)$_2$-complex is $U_{T,Ru\text{-}S}$ = 1/4 $U_{T,High}$ = 0.29 ± 0.02 V which is in the expected range for Ru-complexes.

In the edge case of the symmetric low conductance device, AuPd/Ru(MPTP)(MPTP-SAc/AuNP/Ru(MPTP)(MPTP-SAc/Pt, a weak coupling between the electrodes and the acetyl protected thiol groups is assumed. However, the coupling between the thiol linker of MPTP and the AuNP (Figure 5b, lower part) is strong leading to a pinning of the Ru-complex orbitals to the potential of the AuNP. Here, an applied voltage will shift the potential of the electrodes by +eU/2 and –eU/2, with respect to the potential of the AuNP and the pinned molecular orbitals (Figure 8b). In this case the transition from direct to Fowler-Nordheim tunneling can be achieved only for one of the two tunneling junctions. Furthermore the resulting transition voltage for the Ru(MPTP)(MPTP-SAc)-complex is $U_{T,Ru\text{-}SAc}$ = 1/2 $U_{T,Low}$ = 0.42 ± 0.05 V, which is larger than $U_{T,Ru\text{-}S}$ for the high conductance device based on the Ru(MPTP)$_2$-complex, according to the expectations.

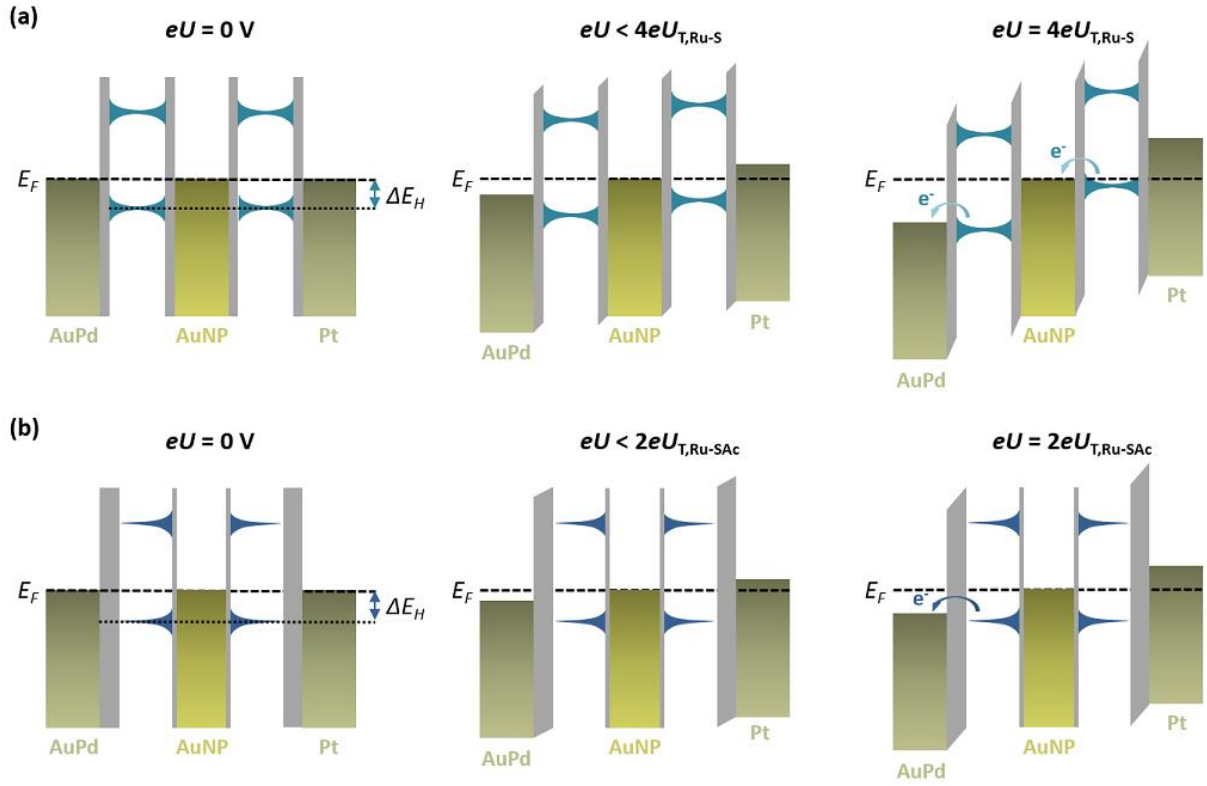

Figure 8. Energy diagrams for double-barrier tunnel junctions formed by (a) the AuPd/Ru(MPTP)$_2$/AuNP/Ru(MPTP)$_2$/Pt junction resulting in a high conductance device with a strong coupling of the Ru-complexes to the AuNP and both electrodes; (b) edge case of a low conductance device AuPd/Ru(MPTP)(MPTP-SAc)/AuNP/Ru(MPTP)(MPTP-SAc)/Pt resulting from Ru-complexes strongly coupled to the AuNP but with only a weak coupling to both electrodes. Based on the optical band gap (defined by the absorption edge, see Figure S6) and ΔE_H the positions of HOMO and LUMO are qualitatively assigned.

3.4. Analysis of the Device Conductance Based on the Single-Channel Landauer Model for Tunneling Transport

Since it is largely accepted that the transition in conductance mechanism from the tunneling to the hopping regime occurs if molecules reach a length of 3 nm to 4 nm, we assume in a first approximation that transport through the here investigated Ru(MPTP)$_2$ complexes can be described by tunneling through a single orbital.[33] We use the single-channel Landauer model which has been proven to be a reliable model to describe tunneling through molecules when $\Delta E_{H,L}$ is significantly larger than the applied potential difference between the electrodes, eU. In this case the energy offset of the frontier orbitals relative to E_F can be correlated to the respective transition voltage:[2,34]

$$\Delta E_{H,L} = \frac{2}{\sqrt{3}}\, eU_T \qquad (1)$$

This correlation can be applied to the Ru(MPTP)$_2$-AuNP devices here under investigation resulting in $\Delta E_{H,Ru\text{-}S}$ = 0.33 ± 0.02 eV and $\Delta E_{H,Ru\text{-}SAc}$ = 0.48 ± 0.06 eV. Reasons for the difference between $\Delta E_{H,Ru\text{-}S}$ and $\Delta E_{H,Ru\text{-}SAc}$ are the different shifts and a different broadening of the molecular orbitals due to a weaker coupling of Ru(MPTP)(MPTP-SAc) to the electrodes compared to Ru(MPTP)$_2$. Derived from the single-channel Landauer formula we use the following relation to calculate the electronic coupling Γ of the frontier orbitals.[34] For $U < 1.5\, \Delta E_{H,L}/e$ and $\Delta E_{H,L} > \Gamma$, the current can be expressed as:

$$I = G_1 U \frac{\Delta E_{H,L}^2}{\Delta E_{H,L}^2 - \left(\frac{eU}{2}\right)^2} \quad (2)$$

By fitting this equation to the *I*/*U*-curves in the voltage regime -0.2 V to +0.2 V the low bias conductance G_1 is obtained. With $\Delta E_{H,L}$ and G_1 the electronic coupling corresponding to the orbital broadening can be calculated:

$$\Gamma = \sqrt{\frac{G_1}{N G_0}} \Delta E_{H,L}, \quad (3)$$

where, G_0 = 77.5 µS is the conductance quantum and *N* the number of molecules building the transport pathway. By assuming *N* = 1 we obtain for the high conductance device $G_{1,\text{Ru-S}}$ = 9.4 ± 0.1 nS, and $\Gamma_{\text{Ru-S}}$ = 3.7 ± 0.3 meV, while the values for the low conductance device are $G_{1,\text{Ru-SAc}}$ = 0.21 ± 0.01 nS and $\Gamma_{\text{Ru-SAc}}$ = 0.8 ± 0.1 meV. Since the low bias conductance and the energy offset determine the orbital broadening, the resulting value for $\Gamma_{\text{Ru-S}}$ is more than four times $\Gamma_{\text{Ru-SAc}}$.

The single-channel Landauer model can be further used to evaluate the experimental device conductance determined at ±1 V according to the method already successfully employed for other single nanoparticle devices.[25,26] In this model, the conductance *G* through a molecule connected to metal electrodes is given by:

$$G = G_0 T_L T_R \, e^{-ßl}. \quad (4)$$

Here, T_L and T_R are the transmission coefficients describing the transport through the left and right molecule/metal interface, *ß* is the electronic decay constant and *l* the length of the molecule.[15] The following values were used for calculations: *l* = 2.2 nm, $T_{\text{Au-SPhen}} = T_{\text{AuPd-SPhen}}$ = 0.4 and $T_{\text{Pt-SPhen}}$ = 0.7. These values are deduced from experimental data on single-molecule devices reported in literature.[36,37] Decay constants for Ru-complexes are found in the range of 2.1 nm^{-1} to 2.7 nm^{-1} and in the range 0.9 nm^{-1} to 1.1 nm^{-1}.[11,12,35,38,39] However, the underlying conductance mechanism in the experiments leading to the low decay constants is interpreted mainly as thermally activated hopping.[11,12] Corresponding to $\Delta E_{\text{H,Ru-S}}$ = 0.33 eV obtained here and assuming hole transport through the HOMO, *ß* = 3.1 ± 0.1 nm^{-1} results for our $Ru(MPTP)_2$ complex and is used in the following

estimations.[15] Considering the double-barrier tunnel junction geometry, the device conductance is calculated using the series formula

$$\frac{1}{G_{dev}} = \frac{1}{G_{Ru,L}} + \frac{1}{G_{Ru,R}} \quad (5)$$

with $G_{Ru,L}$ and $G_{Ru,R}$ the conductance of the Ru-complex on the left and right side of the AuNP. This procedure leads to G = 8.6 nS for the single Ru(MPTP)$_2$-AuNP device and corresponds well to the experimental finding of G = 14 nS. Furthermore, this result suggests that the transport pathway is formed like assumed by single to very few Ru(MPTP)$_2$ complexes at most. It should be mentioned that the thus estimated theoretical device conductance may vary easily by a factor of up to 5, depending on the employed parameter set and the assumed device geometry. Furthermore, the calculated device conductance corresponds to a single-channel conduction and accordingly will increase, if more Ru-complexes are involved. However, so far the application of the single-channel Landauer model was suited best to describe our nanoparticle devices.[24-26]

In the case of the Ru(MPTP)(MPTP-SAc)-AuNP device the molecule/metal interface is formed in the best scenario by a C=O/metal junction with a transmission coefficient of $T_{Au\text{-}CO}$ = 0.06.[40] At the same time the tunneling pathway is increased to an overall length of l = 2.5 nm. Both changes result in a lower conductivity (other scenarios, like a possible but less favorable CH_3/metal junction, would lead to an even lower device conductance). Depending on whether the acetyl end groups remain at one or both molecule/electrode interfaces in the double-barrier tunnel junction the conductivity is calculated to 0.77 nS or 0.40 nS, respectively. On the one hand these results are in excellent agreement with the experimental conductance values for Ru(MPTP)(MPTP-SAc)-AuNP devices given in Figure 5a and indicate that the dominant transport mechanism through single nanoparticle devices functionalized with Ru-terpyridine complexes is tunneling transport via the HOMO. On the other hand, due to the small energy offset from the Fermi level ($\Delta E_{H,Ru\text{-}S}$ = 0.33 eV) and the hysteretic current versus voltage characteristics an additional minor decoherent hopping transport has to be considered. While mere tunneling transport cannot cause a hysteretic behavior, this is possible by charging of a localized molecular orbital due to electron hopping.[6,8,12,41,42] However, the effectivity of

the electron hopping channel is way lower than the effectivity of the tunneling channel since the experimentally obtained device conductance can comprehensively be explained by tunneling transport.

4. Conclusion

In summary, we used hybrid materials based on AuNP functionalized with Ru-terpyridine complexes to assemble nanoscale devices. The electrical characterization of the resulting single $Ru(MPTP)_2$-AuNP devices reveals an electrical robustness, a high stability and a hysteretic current *versus* voltage behavior with an appropriate ON/OFF-ratio which indicates their principle applicability for molecular memories. Thus, the redox-active $Ru(MPTP)_2$-complexes were used to form a voltage-driven solid-state device based on a few or even single functional molecules. The transport behavior through the double-barrier tunnel junctions formed by the Ru-complex ligated AuNP immobilized between two electrodes was described accurately by the single-channel Landauer model for tunneling transport. Furthermore, a quantitative analysis of the experimental data allowed to determine the energy offset of the HOMO and the electronic coupling. It can be concluded that tunneling transport through the HOMO is the predominant mechanism in these solid-state devices while decoherent electron hopping transport has a minor contribution.

ASSOCIATED CONTENT

Supporting Information

The supporting information is available free of charge on the ACS Publications website at DOI:
NMR data and FT-IR spectra of the ligands, nanoelectrode design, AAS and UV-Vis analysis, *I/U* reference measurements, Fowler-Nordheim plots.

AUTHOR INFORMATION

Corresponding Author

*E-mail: s.karthaeuser@fz-juelich.de. Tel: +49 2461 614015
*E-mail: kaulen@fh-aachen.de. Tel: +49-241-600953895

Orcid

Author Contributions

C.K. and S.K.P. synthesized the ligand capped AuNP and performed the spectroscopic characterization. M.M. fabricated the nanoelectronic devices, performed the conductance measurements, and the conductance estimations. The manuscript was written by M.M. and S.K. with contributions of all authors. All authors have given approval to the final version of the manuscript.

Notes

The authors declare no competing financial interest.

ACKNOWLEDGMENTS

The German Research Foundation (DFG Si 609/16-1, Ka 1819/7-1)) supported this work. The authors gratefully acknowledge the technical support of R. Borowski, S. Trellenkamp, and S.K. Potts.

REFERENCES

[1] Xin, N.; Guan, J.; Zhou, C.; Chen, X.; Gu, C.; Li, Y.; Ratner, M.; Nitzan, A.; Stoddart, J. F.; Guo, X. Concepts in the Design and Engineering of Single-Molecule Electronic Devices, *Nat. Rev. Phys.* **2019**, *1*, 211-230.

[2] Vilan, A.; Aswal, D.; Cahen, D. Large-Area, Ensemble Molecular Electronics: Motivation and Challenges. *Chem. Rev.* **2017**, *117*, 4248-4286.

[3] Xiang, D.; Wang, X.; Jia, C.; Lee, T.; Guo, X. Molecular-Scale Electronics: From Concept to Function. *Chem. Rev.* **2016**, *116*, 4318-4440.

[4] Seo, S.; Viet, B. Q.; Hwang, E.; Cho, Y.; Lee, J.; Kawazoe, Y.; Lee. H. Nanoparticle Linker-Controlled Molecular Wire Devices Based on Double Molecular Monolayers. *Small* **2019**, *15*, 1901183.

[5] Tanaka, Y.; Kiguchi, M.; Akita, M. Inorganic and Organometallic Molecular Wires for Single-Molecule Devices. *Chem. Eur. J.* **2017**, *23*, 4741-4749.

[6] Schwarz, F.; Kastlunger, G.; Lissel, F.; Egler-Lucas, C.; Semenov, S. N.; Venkatesan, K.; Berke, H.; Stadler, R.; Lörtscher, E. Field-Induced Conductance Switching by Charge-State Alternation in Organometallic Single-Molecule Junctions. *Nature Nanotech.* **2016**, *11*, 170-176.

[7] Sakamoto, R.; Wu, K.-H.; Matsuoka, R.; Maeda, H.; Nishihara, H. π-Conjugated Bis(terpyridine)metal Complex Molecular Wires. *Chem. Soc. Rev.* **2015**, *44*, 7698-7714.

[8] Luo, L.; Benameur, A.; Brignou, P.; Choi, S. H.; Rigout, S.; Frisbie, C. D. Length and Temperature Dependent Conduction of Ruthenium-Containing Redox-Active Molecular Wires. *J. Phys. Chem. C* **2011**, *115*, 19955-19961.

[9] Breivogel, A.; Kreitner, C.; Heinze, K. Redox and Photochemistry of Bis(terpyridine)ruthenium(II) Amino Acids and Their Conjugates – from Understanding to Applications. *Eur. J. Inorg. Chem.* **2014**, 5468-5490.

[10] Tuccitto, N.; Ferri, V.; Cavazzini, M.; Quici, S.; Zhavnerko, G.; Licciardello, A.; Rampi, M. A. Highly Conductive 40-nm-long Molecular Wires Assembled by Stepwise Incorporation of Metal Centres. *Nature Mater.* **2009**, *8*, 41-46.

[11] Chappell, S.; Brooke, C.; Nichols, R. J.; Cook, L. J. K.; Halcrow, M.; Ulstrup, J.; Higgins, S. J. Evidence for a Hopping Mechanism in Metal/Single Molecule/Metal Junctions Involving Conjugated Metal-Terpyridyl Complexes. *Faraday Discuss.* **2016**, *193*, 113-131.

[12] Higgins, S. J.; Nichols, R. J. Metal/Molecule/Metal Junction Studies of Organometallic and Coordination Complexes; What Can Transition Metals Do for Molecular Electronics? *Polyhedron* **2018**, *140*, 25-34.

[13] Davidson, R.; Liang, J.-H.; Milan, D. C.; Mao, B.-W.; Nichols, R. J.; Higgins, S. H.; Yufit, D. S.; Beeby, A.; Low, P. J. Synthesis, Electrochemistry, and Single-Molecule Conductance of Bimetallic 2,3,5,6-Tetra(pyridine-2yl)pyrazine-Based Complexes. *Inorg. Chem.* **2015**, *54*, 5487-5494.

[14] Xie, Z.; Baldea, I.; Smith, C. E.; Wu, Y.; Frisbie, C. D. Experimental and Theoretical Analysis of Nanotransport in Oligophenylene Dithiol Junctions as a Function of Molecular Length and Contact Work Function. *ACS Nano* **2015**, *9*, 8022-8036.

[15] Karthäuser, S. Control of Molecule-Based Transport for Future Molecular Devices. *J. Phys.: Condens. Matter* **2011**, *23*, 013001.

[16] Pal, P.; Mukherjee, S.; Maity, D.; Baitalik, S. Synthesis, Photophysics, and Switchable Luminescence Properties of a New Class of Ruthenium(II)–Terpyridine Complexes Containing Photoisomerizable Styrylbenzene Units. *ACS Omega*. **2018**, *3*, 14526-14537.

[17] Winter, A.; Hoeppener, S.; Newkome, G. R.; Schubert, U. S. Terpyridine-Functionalized Surfaces: Redox-Active, Switchable, and Electroactive Nanoarchitectures. *Adv. Mater.* **2011**, *23*, 3484-3498.

[18] Lee, J.; Chang, H.; Kim, S.; Bang, G. S.; Lee, H. Molecular Monolayer Nonvolatile Memory with Tunable Molecules. *Angew. Chem. Int. Ed*. **2009**, *48*, 8501-8504.

[19] Seo, S.; Min, M.; Lee, J.; Lee, T.; Choi, S.-Y.; Lee, H. Solution-Processed Reduced Graphene Oxide Films as Electronic Contacts for Molecular Monolayer Junctions. *Angew. Chem. Int. Ed.* **2012**, *51*, 108-112.

[20] Li, J.-C.; Wu, J.-Z.; Gong, X. Conductance Switching and Photovoltaic Effect of Ru(II) Complex Molecular Junctions: Role of Complex Properties and the Metal/Molecule Interface. *J. Phys. Chem. Lett.* **2014**, *5*, 1017-1021.

[21] Seo, K.; Konchenko, A. V.; Lee, J.; Bang, G. S.; Lee, H. Molecular Conductance Switch-On of Single Ruthenium Complex Molecules. *J. Am. Chem. Soc.* **2008**, *130*, 2553-2559.

[22] Winter, A.; Hager, M. D.; Newkome, G. R.; Schubert, U. S. The Marriage of Terpyridines and Inorganic Nanoparticles: Synthetic Aspects, Characterization Techniques, and Potential Applications. *Adv. Mater*. **2011**, *23*, 5728-5748.

[23] Manheller, M.; Karthäuser, S.; Waser, R.; Blech, K.; Simon, U. Electrical Transport through Single Nanoparticles and Nanoparticle Arrays. *J. Phys. Chem. C* **2012**, *116*, 20657-20665.

[24] Babajani, N.; Kowalzik, P.; Waser, R.; Homberger, M.; Kaulen, C.; Simon, U.; Karthäuser, S. Electrical Characterization of 4-Mercaptophenylamine Capped Nanoparticles in a Heterometallic Nanoelectrode Gap. *J. Phys. Chem. C* **2013**, *117*, 22002-22009.

[25] Babajani, N.; Kaulen, C.; Homberger, M.; Mennicken, M.; Waser, R.; Simon, U.; Karthäuser, S. Directed Immobilization of Janus-AuNP in Heterometallic Nanogaps: a Key Step Toward Integration of Functional Molecular Units in Nanoelectronics. *J. Phys. Chem. C* **2014**, *118*, 27142−27149.

[26] Mennicken, M.; Peter, S. K.; Kaulen, C.; Simon, U.; Karthäuser, S. Controlling the Electronic Contact at the Terpyridine/Metal Interface. *J. Phys. Chem. C* **2019**, *123*, 21367-21375.

[27] Manheller, M.; Trellenkamp, S.; Waser, R.; Karthäuser, S. Reliable Fabrication of 3nm Gaps between Nanoelectrodes by Electron-beam Lithography. *Nanotechnology* **2012**, *23*, 125302.

[28] Tang, J.; Wang, Y.; Nuckolls, C.; Wind, S. Chemically Responsive Molecular Transistors Fabricated by Self-Aligned Lithography and Chemical Self-assembly, *J. Vac. Sci. Technol. B* **2006**, *24*, 3227-3229.

[29] Turkevich, J.; Stevenson, P. C.; Hillier, J. A Study of the Nucleation and Growth Processes in the Synthesis of Colloidal Gold. *Discuss. Faraday Soc.* **1951**, *11*, 55-75.

[30] Peter, S. K.; Kaulen, C.; Hoffmann, A.; Ogieglo, W.; Karthäuser, S.; Homberger, M.; Herres-Pawlis, S.; Simon, U. Stepwise Growth of Ruthenium Terpyridine Complexes on Au Surfaces. *J. Phys. Chem. C* **2019**, *123*, 6537-6548.

[31] Ziessel, R.; Grossenhenny, V.; Hissler, M.; Stroh, C. Cis-[Ru(2,2‘:6‘,2‘ ‘-terpyridine)(DMSO)Cl_2]: Useful Precursor for the Synthesis of Heteroleptic Terpyridine Complexes under Mild Conditions. *Inorg. Chem.* **2004**, *43*, 4262-4271.

[32] Pandey, R. K.; Chakraborty, C.; Rana, U.; Moriyama, U.; Higuchi, M. An Insight into Ion-Conduction Phenomenon of Gold Nanocluster Ligand Based Metallosupramolecular Polymers. *J. Mater. Chem. A*, **2016**, *4*, 4398-4401.

[33] Choi, S. H.; Kim, B. S.; Frisbie, C. D. Electrical Resistance of Long Conjugated Molecular Wires. *Science* **2008**, *320*, 1482–1486.

[34] Smith, C. E.; Xie, Z.; Baldea, I.; Frisbie, C. D. Work Function and Temperature Dependence of Electron Tunneling trough an N-Type Perylene Diimide Molecular Junction with Isocyanide Surface Linkers. *Nanoscale* **2018**, *10*, 964-975.

[35] Liu, K.; Wang, X.; Wang, F. Probing Charge Transport of Ruthenium-Complex-Based Molecular Wires at the Single-Molecule Level. *ACS Nano* **2008**, *2*, 2315-2323.

[36] Seth, C.; Kaliginedi, V.; Suravarapu, S.; Reber, D.; Hong, W.; Wandlowski, T.; Lafolet, F.; Broekmann, P.; Royal, G.; Venkatramani, R. Conductance in a Bisterpyridine Based Single Molecular Breadboard Circuit. *Chem. Sci.* **2017**, *8*, 1576-1591.

[37] Kaliginedi, V.; Moreno-García, P.; Valkenier, H.; Hong, W.; García-Suárez, V. M.; Buiter, P.; Otten, J. L. H.; Hummelen, J. C.; Lambert, C. J.; Wandlowski, T. Correlations between Molecular Structure and Single-Junction Conductance: A Case Study with Oligo(phenylene-ethynylene)-Type Wires. *J. Am. Chem. Soc.* **2012**, *134*, 5262-5275.

[38] Stadler, A.-M.; Puntoriero, F.; Nastasi, F.; Campagna, S.; Lehn, J.-M. Ru^{II} Multinuclear Metallosupramolecular Rack-Type Architectures of Polytopic Hydrazone-Based Ligands: Synthesis, Structural Features, Absorption Spectra, Redox Behavior, and Near-Infrared Luminescence. *Chem. Eur. J.* **2010**, *16*, 5645-5660.

[39] Fabre, M.; Bonvoisin, J. Electronic and Magnetic Communication in Mixed-Valent and Homovalent Ruthenium Complexes Containing Phenylcyanamide Type Bridging Ligands. *J. Am. Chem. Soc.* **2007**, *129*, 1434-1444.

[40] Chen, F.; Li, X.; Hihath, J.; Huang, Z.; Tao, N. Effect of Anchoring Groups on Single-Molecule Conductance: Comparative Study of Thiol-, Amine-, and Carboxylic-Acid-Terminated Molecules. *J. Am. Chem. Soc.* **2006**, *128*, 15874-15881.

[41] Kastlunger, G.; Stadler, R. Density Functional Theory Based Direct Comparison of Coherent Tunneling and Electron Hopping in Redox-Active Single-Molecule Junctions. *Phys. Rev. B* **2015**, *91*, 125410.

[42] Sowa, J. K.; Mol, J. A.; Briggs, A. D.; Gauger, E. M. Beyond Marcus Theory and the Landauer-Büttiker Approach in Molecular Junctions: A Unified Framework. *J. Chem. Phys.* **2018**, *149*, 154112.

TOC Graphic